Building up low-complexity spectrally-efficient Terabit superchannels by receiver-side duobinary shaping

Jianqiang Li,* Martin Sjödin, Magnus Karlsson, and Peter A. Andrekson

Photonics Laboratory, Department of Microtechnology and Nanoscience, Chalmers University of Technology, Gothenburg SE-412 96, Sweden

jqjqlee@gmail.com

Abstract: Recently, an increasing interest has been put on spectrally-efficient multi-carrier superchannels for beyond 100G. Apart from orthogonal frequency-division multiplexing (OFDM) and Nyquist wavelength-division multiplexing (WDM), another low-complexity WDM approach based on transmitter-side pre-filtering and receiver-side duobinary shaping is proposed to build up multi-carrier superchannels. This approach is referred to as receiver-side duobinary-shaped WDM (RS-DBS-WDM). Generation and transmission of a 1.232-Tbit/s 11-carrier superchannel is experimentally demonstrated. The superchannel signal can be well fit inside the passband of multiple 300-GHz reconfigurable optical add and drop multiplexers (ROADMs). In the superchannel scenario, the proposed RS-DBS-WDM is qualitatively compared with OFDM and Nyquist-WDM in terms of implementation complexity. In sum, the proposed RS-DBS-WDM approach features high transceiver analog-bandwidth efficiency, high spectral-efficiency, the absence of specific spectral manipulation, compatibility with conventional WDM technologies and coherent detection algorithms, and comparable implementation penalty.

OCIS codes: (060.1660) Coherent communications; (060.2330) Fiber optics communication; (060.4230) Multiplexing.

References and links

1. X. Liu, S. Chandrasekhar, B. Zhu, P. J. Winzer, A. H. Gnauck, and D. W. Peckham, "448-Gb/s reduced-guard-interval CO-OFDM transmission over 2000 km of ultra-large-area fiber and five 80-GHz-grid ROADMs," J. Lightwave Technol. **29**(4), 483–490 (2011).
2. Y. Ma, Q. Yang, Y. Tang, S. Chen, and W. Shieh, "1-Tb/s single-channel coherent optical OFDM transmission over 600-km SSMF fiber with subwavelength bandwidth access," Opt. Express **17**(11), 9421–9427 (2009).
3. A. Sano, E. Yamada, H. Masuda, E. Yamazaki, T. Kobayashi, E. Yoshida, Y. Miyamoto, R. Kudo, K. Ishihara, and Y. Takatori, "No-guard-interval coherent optical OFDM for 100-Gb/s long-haul WDM transmission," J. Lightwave Technol. **27**(16), 3705–3713 (2009).
4. S. Chandrasekhar, X. Liu, B. Zhu, and D. W. Peckham, "Transmission of a 1.2 Tb/s 24-carrier no-guard-interval coherent OFDM superchannel over 7200-km of ultra-large-area fiber," presented at the ECOC 2009, Vienna, Austria, Sep. 20–24, 2009, Paper PD2.6.
5. J. Yu, Z. Dong, X. Xiao, Y. Xia, S. Shi, C. Ge, W. Zhou, N. Chi, and Y. Shao, "Generation of 112 coherent multi-carriers and transmission of 10 Tb/s (112x100Gb/s) single optical OFDM superchannel over 640 km SMF," in Proc. OFC2011, Mar. 2011, Paper PDPA6.
6. J. Yu, Z. Dong, J. Zhang, X. Xiao, H.-C. Chien, and N. Chi, "Generation of coherent and frequency-locked multi-carriers using cascaded phase modulators for 10Tb/s optical transmission," J. Lightwave Technol. **30**(4), 458–465 (2012).
7. G. Bosco, A. Carena, V. Curri, P. Poggiolini, and F. Forghieri, "Performance limits of Nyquist-WDM and CO-OFDM in high-speed PM-QPSK systems," IEEE Photon. Technol. Lett. **22**(15), 1129–1131 (2010).
8. R. Schmogrow, M. Winter, M. Meyer, D. Hillerkuss, S. Wolf, B. Baeuerle, A. Ludwig, B. Nebendahl, S. Ben-Ezra, J. Meyer, M. Dreschmann, M. Huebner, J. Becker, C. Koos, W. Freude, and J. Leuthold, "Real-time Nyquist pulse generation beyond 100 Gbit/s and its relation to OFDM," Opt. Express **20**(1), 317–337 (2012).

#161326 - $15.00 USD Received 11 Jan 2012; revised 23 Feb 2012; accepted 19 Mar 2012; published 19 Apr 2012

9. X. Zhou, L. E. Nelson, P. Magill, R. Isaac, B. Zhu, D. W. Peckham, P. I. Borel, and K. Carlson, "PDM-Nyquist-32QAM for 450-Gb/s per-channel WDM transmission on the 50 GHz ITU-T grid," J. Lightwave Technol. **30**(4), 553–559 (2012).
10. R. Cigliutti, E. Torrengo, G. Bosco, N. P. Caponio, A. Carena, V. Curri, P. Poggiolini, Y. Yamamoto, T. Sasaki, and F. Forghieri, "Transmission of 9×138Gb/s prefiltered PM-8QAM signals over 4000 km of pure silica-core fiber," J. Lightwave Technol. **29**(15), 2310–2318 (2011).
11. G. Gavioli, E. Torrengo, G. Bosco, A. Carena, V. Curri, V. Miot, P. Poggiolini, M. Belmonte, F. Forghieri, C. Muzio, S. Piciaccia, A. Brinciotti, A. L. Porta, C. Lezzi, S. Savory, and S. Abrate, "Investigation of the impact of ultra-narrow carrier spacing on the transmission of a 10-carrier 1Tb/s superchannel," in Proc. OFC 2010, San Diego, CA, March 2010, Paper OThD3.
12. J. Li, E. Tipsuwannakul, T. Eriksson, M. Karlsson, and P. A. Andrekson, "Approaching Nyquist limit in WDM systems by low-complexity receiver-side duobinary shaping," to be published in J. Lightwave Technol.
13. J. G. Proakis, *Digital Communications,* 4th ed. (New York McGraw-Hill, 2001).
14. G. D. Forney, Jr., "Maximum likelihood sequence estimation of digital sequences in the presence of intersymbol interference," IEEE Trans. Inf. Theory **18**(3), 363–378 (1972).
15. H. Kobayashi, "Correlative level coding and maximum likelihood decoding," IEEE Trans. Inf. Theory **17**(5), 586–594 (1971).
16. N. Alic, G. C. Papen, R. E. Saperstein, R. Jiang, C. Marki, Y. Fainman, S. Radic, and P. A. Andrekson, "Experimental demonstration of 10 Gb/s NRZ extended dispersion-limited reach over 600km-SMF link without optical dispersion compensation," presented in OFC 2006, Anaheim, CA, March 2006, paper OWB7.
17. N. Alic, M. Karlsson, M. Skold, O. Milenkovic, P. A. Andrekson, and S. Radic, "Joint statistics and MLSD in filtered incoherent high-speed fiber-optic communications," J. Lightwave Technol. **28**(10), 1564–1572 (2010).
18. J. Li, E. Tipsuwannakul, M. Karlsson, and P. A. Andrekson, "Low-complexity duobinary signaling and detection for sensitivity improvement in Nyquist-WDM coherent system," presented in OFC 2012, Los Angeles, CA, March 2012, Paper OM3H.2.
19. I. Lyubomirsky, "Quadrature duobinary modulation for 100G transmission beyond the Nyquist limit," in Proc. OFC 2010, San Diego, CA, March 2010, Paper OThM4.
20. I. Lyubomirsky, "Quadrature duobinary for high-spectral efficiency 100G transmission," J. Lightwave Technol. **28**(1), 91–96 (2010).
21. J. Li, Z. Tao, H. Zhang, W. Yan, T. Hoshida, and J. C. Rasmussen, "Spectrally efficient quadrature duobinary coherent systems with symbol-rate digital signal processing," J. Lightwave Technol. **29**(8), 1098–1104 (2011).
22. R. Nagarajan, D. Lambert, M. Kato, V. Lal, G. Goldfarb, J. Rahn, M. Kuntz, J. Pleumeekers, A. Dentai, H. -S. Tsai, R. Malendevich, M. Missey, K. -T. Wu, H. Sun, J. McNicol, J. Tang, J. Zhang, T. Butrie, A. Nilsson, M. Reffle, F. Kish, and D. Welch, "10 channel, 100Gbit/s per channel, dual polarization, coherent QPSK, monolithic InP receiver photonic integrated circuit," in Proc. OFC2011, Mar. 2011, Paper OML7.
23. S. Chandrasekhar and X. Liu, "Experimental investigation on the performance of closely spaced multi-carrier PDM-QPSK with digital coherent detection," Opt. Express **17**(24), 21350–21361 (2009).
24. J.-X. Cai, C. R. Davidson, A. Lucero, H. Zhang, D. G. Foursa, O. V. Sinkin, W. W. Patterson, A. N. Pilipetskii, G. Mohs, and N. S. Bergano, "20 Tbit/s transmission over 6860 km with sub-Nyquist channel spacing," J. Lightwave Technol. **30**(4), 651–657 (2012).
25. K. Horikoshi, T. Kobayashi, S. Yamanaka, E. Yamazaki, A. Sano, E. Yoshida, and Y. Miyamoto, "Spectrum-narrowing tolerant 171-Gbit/s PDM-16QAM transmission over 1,200 km using maximum likelihood sequence estimation," in Proc. ECOC 2011, Paper We.10.P1.73.
26. M. Selmi, Y. Jaouën, and P. Ciblat, "Accurate digital frequency offset estimator for coherent PolMux QAM transmission systems," in Proc. ECOC 2009, Sep. 2009, Paper P3.08.
27. S. J. Savory, "Digital coherent optical receivers: algorithms and subsystems," IEEE J. Sel. Top. Quantum Electron. **16**(5), 1164–1179 (2010).
28. V. M. Eyuboglu and S. U. Qureshi, "Reduced-state sequence estimation for coded modulation on intersymbol interference channels," IEEE J. Sel. Areas Comm. **7**(6), 989–995 (1989).
29. S. Olcer, "Reduced-state sequence detection of multilevel partial-response signals," IEEE Trans. Commun. **40**(1), 3–6 (1992).

1. Introduction

Recently, there is an increasing attention devoted to multi-carrier superchannels to address the great implementation challenges for transmission systems beyond 100G. At the same time, there is also a strong motivation on enhancing the spectral-efficiency in order to scale up the total capacity and reduce the cost per bit. From a spectral multiplexing point of view, two major competitive technologies for forming spectrally-efficient multi-carrier superchannels can be identified so far. One is the orthogonal frequency-division multiplexing (OFDM) technology which makes use of subcarrier orthogonality to allow for spectral overlapping [1–6]. A diversity of implementing methods has been proposed, such as electro-optical hybrid OFDM or namely multi-band OFDM [1,2], and all-optical OFDM or namely no-guard-

#161326 - $15.00 USD Received 11 Jan 2012; revised 23 Feb 2012; accepted 19 Mar 2012; published 19 Apr 2012

interval OFDM (NGI-OFDM) [3–6]. The other is referred to as Nyquist wavelength-division multiplexing (WDM) that bases its innovation on WDM systems [7–10]. With the transmitted signal spectrum in each individual carrier shaped into a rectangular profile, it is possible to achieve a near-baud-rate carrier spacing. With respect to OFDM, Nyquist-WDM has relaxed requirements on the receiver hardware in terms of the analog bandwidth and the sampling speed of the analog-to-digital converters (ADCs) [7]. However, specific Nyquist filters are required in either the electrical [8,9] or optical [10,11] domain, which imposes much complexity on the transmitter side. From a smooth upgrading and fast deployment point of view, it is favorable to apply existing WDM components and engineering techniques without requiring the long-term advance of new specific components or technologies.

More recently, we developed a general receiver-side partial-response shaping technique in the digital domain for strongly-pre-filtered WDM systems with coherent detection [12]. In this technique, the receiver-side spectral shaping can relax the heavy burden and stringent requirement on the transmitter-side spectral shaping, and permit the use of the conventional transmitters and mature WDM components. After partial-response shaping, the well-known maximum likelihood sequence detection (MLSD) [13–17] is applied to detect the shaped signal with optimum performance. In such pre-filtered WDM systems with a channel spacing of around the baud rate, duobinary shaping has been experimentally proved as a good partial-response shaping option in terms of the tradeoff between the complexity and performance [12,18]. In fact, the selection of the duobinary response was inspired by the quadrature duobinary systems originally investigated in [19–21]. In this paper, the duobinary shaping is considered since we here focus on the multi-carrier superchannel scenario with a carrier spacing of around baud rate. This technique is referred to as receiver-side duobinary-shaped WDM (RS-DBS-WDM). In this paper, the RS-DBS-WDM system is exploited as another competitive solution to building up spectrally-efficient Terabit multi-carrier superchannels, with respect to OFDM and Nyquist-WDM. The generation and transmission of a 1.232 Tb/s RS-DBS-WDM superchannel are experimentally demonstrated. The 1.232 Tb/s superchannel is composed of eleven 112 Gb/s polarization-multiplexed quadrature phase-shift keying (PM-QPSK) carriers pre-filtered by regular WDM components (i.e. optical interleavers in this paper). Since it occupies a 10-dB bandwidth of about 280 GHz, the superchannel signal can be fit inside the passband of multiple concatenated 300-GHz wavelength selective switches (WSSs) with a sufficient margin. In particular, a multiplier-free operation can be achieved during the MLSD of duobinary-shaped QPSK signals, which makes the complexity increment introduced by MLSD be small as compared to the hard-decision detection. Finally, three potential solutions to forming superchannels (i.e. OFDM, Nyquist-WDM, and RS-DBS-WDM) are compared.

2. Building up RS-DBS-WDM superchannels

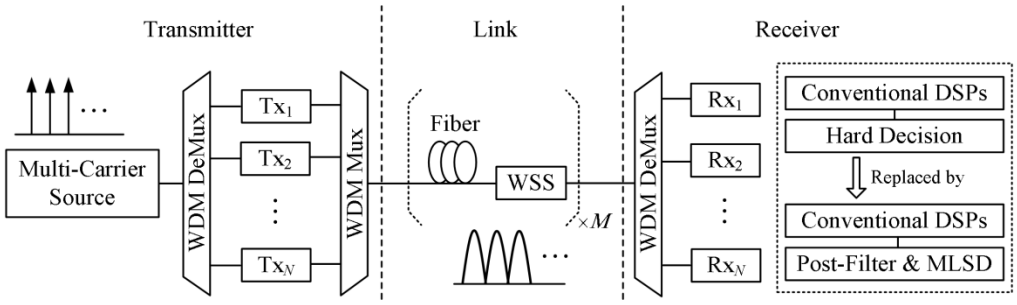

Fig. 1. Schematic setup of a RS-DBS-WDM superchannel system.

The schematic setup of a RS-DBS-WDM superchannel system is shown in Fig. 1. Since the RS-DBS-WDM can be considered as an ultra-dense form of WDM, the setup is the same as in

#161326 - $15.00 USD Received 11 Jan 2012; revised 23 Feb 2012; accepted 19 Mar 2012; published 19 Apr 2012

a conventional WDM system, as seen in Fig. 1. On the transmitter side, either a multi-carrier generator or multiple discrete lasers are used to provide multiple continuous-wave (CW) carriers. A multi-carrier generator is preferred since it ensures a stable and practical frequency separation among a large number of carriers. The carrier frequency spacing is set to be around the baud rate of each individual carrier. As explained and demonstrated in [12,18], no special spectral manipulation is needed due to the proposed receiver-side adaptive duobinary shaping in the digital domain. Therefore, the mature WDM components (e.g. arrayed waveguide gratings, AWGs, and optical interleavers) can be directly used to strongly pre-filter the signal in each individual carrier and multiplex them together to form the superchannel. The compatibility with these conventional WDM components helps to reduce the insertion loss and thereby to improve the delivered optical signal-to-noise ratio (OSNR) from the transmitters. In future flexible optical networks, the entire superchannel is routed over multiple WSSs as a single entity. On the receiver side, one WDM demultiplexer first separates the carriers and then feeds them into multiple parallel digital coherent receivers. In each digital coherent receiver, most of the conventional digital signal processing (DSP) blocks are remained without any modifications. The only difference is that the combination of the post-filter and the MLSD replaces the conventional hard decision circuits [12,18]. For the practical implementation of Terabit superchannels, high-density and large-scale photonic integration is in high demand for low cost, small footprint, and low power dissipation. It can be seen from Fig. 1 that the superchannel setup is compatible with the currently-available Terabit photonic integrated circuits without any specific designs [22].

3. Experiments

3.1 Experimental setup and DSP algorithms

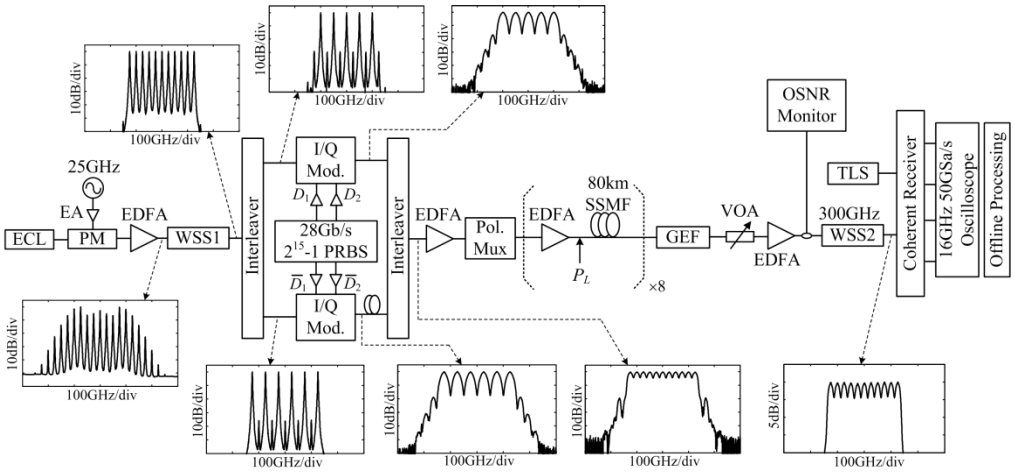

Fig. 2. Setup and optical spectra in the 1.232 Tbit/s PM-QPSK RS-DBS-WDM superchannel experiment.

The experimental setup and the corresponding optical spectra in several monitor points are shown in Fig. 2. The total capacity of the superchannel is targeted to 1.232 Tbit/s in support of future 1T Ethernet transport with ~20% soft-decision forward error correction (FEC) overhead. The superchannel consists of eleven 25 GHz-spaced carriers each of which carries a 112 Gbit/s PM-QPSK signal. The 11 continuous-wave (CW) carriers were generated from a single narrow-linewidth external-cavity laser (ECL) at 1550.92 nm by using one phase modulator (PM) with a low half-wave voltage ($V\pi \approx 4V$). The PM was driven by a boosted 25 GHz RF clock signal with a peak-to-peak voltage of ~17V. After the PM, more than 15 carriers were produced, and the central 11 carriers were selected and gain-equalized by a configurable WSS (a Finisar WaveShaper in our experiments). After the WSS, the maximum

#161326 - $15.00 USD Received 11 Jan 2012; revised 23 Feb 2012; accepted 19 Mar 2012; published 19 Apr 2012

power difference is within 0.3 dB showing good power flatness. This multi-carrier generation method by strongly-driven optical external modulators has been successfully used in the previous literatures [1,3,5,6,9,23], despite the possible presence of spurious components induced by the nonlinearities of the modulator and its drivers. Note that the produced carriers by this means are both frequency- and phase-locked, whereas phase locking is not indispensable for RS-DBS-WDM. These 11 CW carriers were then separated into two groups by a 25/50 GHz optical interleaver for even and odd carriers. Two I/Q modulators driven by two pairs of decorrelated 28 Gbit/s 2^{15}-1 pseudo-random bit sequence (PRBS) data were used to generate optical QPSK signals for even and odd carriers, respectively. The differential delay between PRBS data D_1 and D_2 is 2^{14} bits (i.e. roughly half word length). After the even and odd decorrelation by optical delay lines (a relative delay of 278 symbols), the 28 Gbaud QPSK signals in even and odd carriers were strongly-filtered and combined together by another 25/50GHz optical interleaver. Figure 3 illustrates the contrast between the 28 Gbaud QPSK spectrum and the transfer function of the commercial 25/50 GHz optical interleaver. It can be seen that the QPSK signal was aggressively filtered in order to fit into the 25 GHz carrier spacing with acceptable linear crosstalk. After polarization multiplexing with a relative delay of 180 symbols, the final 11-carrier 1.232 Tbit/s superchannel signal was launched to the fiber link without inline dispersion management. The fiber link was built up in straight line using eight 80 km standard single-mode fiber (SSMF) spans with Erbium-doped fiber amplifiers (EDFAs) only. The launched optical power (P_L) into the SSMF spool in each span was the same. A gain-equalization filter (GEF) was placed after the link to compensate for the gain slope of inline EDFAs. Limited equipment availability only permitted us to implement 640 km SSMF transmissions in a straight line, leaving a large amount of OSNR margin (>10 dB w.r.t. the soft-decision FEC threshold) at the optimal launched optical power. We inserted a variable optical attenuator (VOA) before the pre-EDFA to load more amplified spontaneous emission (ASE) noise at the receiver. One 300 GHz WSS was used to suppress the ASE noise and select the 1.232 Tbit/s superchannel as a single entity. Coherent detection of the 11 carriers was implemented one by one through a commercial integrated coherent receiver in a polarization- and phase-diversity configuration. The wavelength of the tunable laser source (TLS) was tuned to determine which carrier was detected. Finally, the detected electrical signals were digitized and captured with 3×10^6 samples each by a 50 GSa/s digital sampling oscilloscope with a 16 GHz analog bandwidth for offline processing.

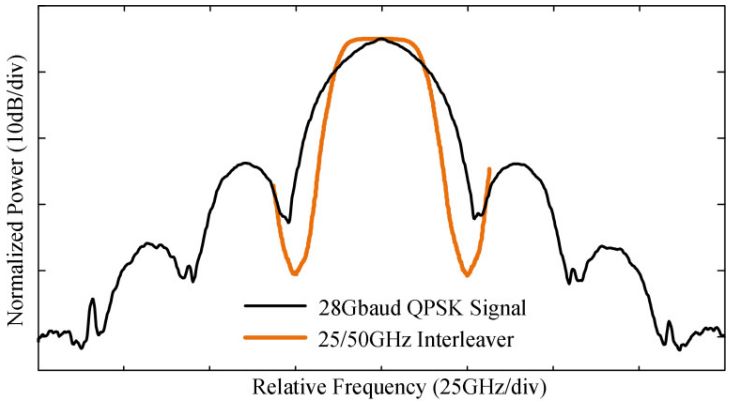

Fig. 3. 28 Gbaud QPSK spectrum and the transfer function of the used 25/50GHz optical interleaver.

As seen in Fig. 4, the DSP blocks in a conventional PM-QPSK coherent receiver [21] were all remained without any modification. The only difference was that the hard decision circuits were substituted by a post-filter and MLSD on each signal quadrature path in each polarization. As explained in [12], minimum modification was made on the algorithms in our

#161326 - $15.00 USD Received 11 Jan 2012; revised 23 Feb 2012; accepted 19 Mar 2012; published 19 Apr 2012

proposed DSPs, unlike [24,25]. The entire DSP structure exhibits a simple feed-forward structure, which enables the convenient reconfiguration in the digital coherent receiver. For instance, hard decision is commonly used in conventional WDM systems, while it can be easily switched to the post-filter and MLSD in the presence of aggressive filtering. The algorithms are described in brief as follows. After I/Q imbalance compensation, the four sample streams were resampled to 2 samples per symbol. The electronic dispersion compensation (EDC) based on static time-domain equalization was performed to compensate for the whole accumulated dispersion in the fiber link. The adaptive equalization and polarization demultiplexing were performed by four butterfly-structured 15-tap *T*/2-spaced finite impulse-response (FIR) filters adapted by the classic constant-modulus algorithm (CMA). It has been demonstrated in [12] that CMA works well even in the presence of more aggressive pre-filtering. Carrier recovery was done including the frequency offset estimation based on the fast Fourier transform (FFT) method [26] and carrier phase estimation based on 4th-power Viterbi-Viterbi algorithm [27]. Note that all the DSP parameters were kept fixed for every case, such as the tap number and step size of CMA-based FIR filters, averaging window size of carrier phase estimation. After the above conventional DSP, the duobinary post-filter and the MLSD were applied on each individual signal quadrature path of each polarization where the signal has a duobinary-shaped 2-ary pulse-amplitude modulation (2PAM) format. Therefore, the MLSD based on the Viterbi algorithm only contains two states. In particular, we applied an improved MLSD algorithm with multiplier-free operations, which is elaborated in Appendix. With this improved algorithm, both the post-filter and MLSD can be multiplier free, indicating a small DSP complexity increment with respect to the hard decision circuits.

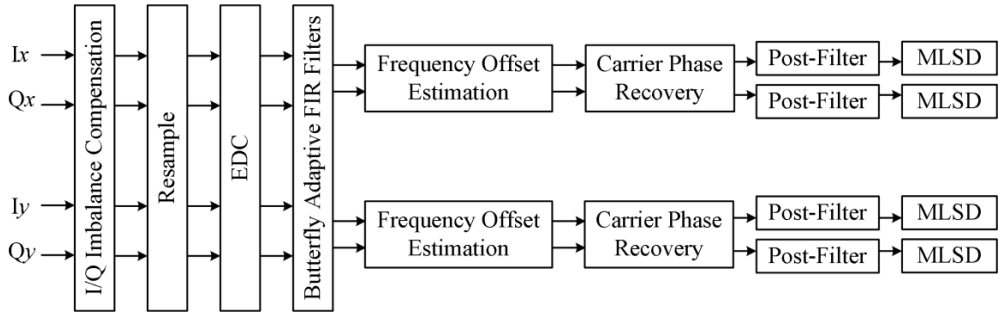

Fig. 4. DSP flow chart in each individual digital coherent receiver for each carrier.

3.2 B2B performance

The experimental results at B2B are shown in Fig. 5. In this paper, the OSNR is defined with 0.1 nm noise reference bandwidth. Firstly, the WSS1 was configured to pass only one carrier and meanwhile the interleaver after the I/Q modulator was bypassed. In this case, the performance of the conventional single-carrier 112 Gbit/s PM-QPSK was measured (empty circles). Since there is no strong pre-filtering, hard decision can be applied instead. As compared to the theoretical limit, there is a typical 1 dB OSNR penalty for bit-error rate (BER) = 10^{-3}. Secondly, aggressive optical filtering was applied on the single-carrier 112 Gbit/s PM-QPSK signal by inserting the 25/50GHz interleaver after the QPSK modulation. In this case, the post-filter and MLSD were activated to replace the hard decision. The single-carrier 28 Gbaud PM-QPSK signal passing the 25/50GHz interleaver only suffers from ~0.7 dB OSNR penalty (empty squares). In contrast, the OSNR penalty increases to ~1.5 dB if the hard decision is applied (filled squares). Thirdly, since the linear crosstalk only originates from its most adjacent carriers in practical systems, we turned on the two most adjacent carriers by configuring WSS1 in order to investigate the impact of the inter-carrier linear crosstalk. Another 1.1 dB OSNR penalty appears (empty triangles). In total, there is about 1.8

#161326 - $15.00 USD Received 11 Jan 2012; revised 23 Feb 2012; accepted 19 Mar 2012; published 19 Apr 2012

dB OSNR penalty for BER = 10^{-3} in the presence of both aggressive filtering and linear crosstalk. In the 11-carrier case, there is an extra OSNR penalty of ~0.8 dB. This is because the optical QPSK signal in even or odd carriers were generated using a single I/Q modulator, thereby suffering from an additional amount of linear crosstalk. However, this will not happen in practical systems. In contrast, the BER is unable to reach 10^{-3} if we used direct hard decision (filled triangles). Referring to the four curves with triangles and squares, one can conclude that a larger performance improvement is obtained by the post-filter and MLSD in the presence of linear crosstalk (i.e. 3-carrier case) as compared to the 1-carrier case. Note that these results are consistent with those in [12,18] where the WaveShapers programmed with super Gaussian profile were used to perform the aggressive pre-filtering, indicating the feasibility of using commercial WDM components.

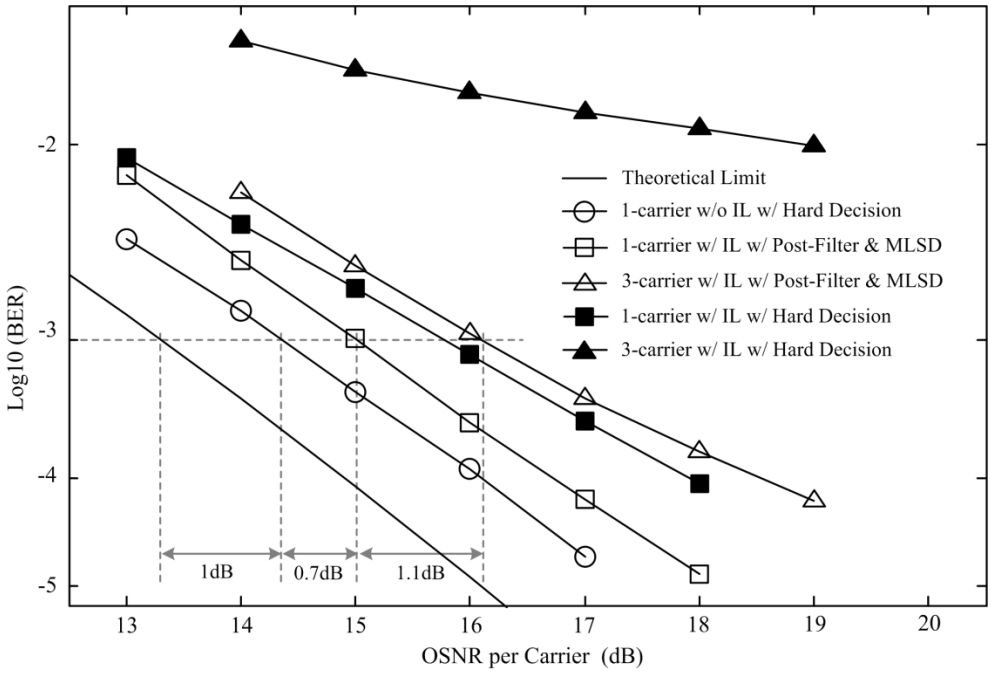

Fig. 5. B2B performance as a function of OSNR for different cases. IL: interleaver.

3.3 Fiber transmission performance

The experimental results for 640 km SSMF transmission of 1.232 Tbit/s 11-carrier PM-QPSK RS-DBS-WDM superchannel are shown in Fig. 6. As mentioned earlier, a large amount of OSNR margin was left merely after 640 km fiber transmission, we intentionally loaded an additional amount of ASE noise to obtain ~30 dB received OSNR for the entire superchannel (i.e. ~19.6 dB OSNR per carrier). The BER in Fig. 6 was obtained by averaging the BERs of all 11 carriers. The optimal launched total optical power of the 1.232 Tbit/s superchannel signal is 10 dBm (i.e. –0.6 dBm per carrier). After fiber transmission, there is still a large performance improvement owing to the post-filter and MLSD. The performance improvement can be intuitively observed from the constellations in Fig. 6. These two constellations come from the central carrier (6th carrier) at a launched power of 10 dBm before and after post-filtering, respectively. After post-filtering, the signal had a much clearer constellation despite an increased constellation density. After 640 km fiber transmission at 10-dBm launched optical power (i.e. ~19.6 dB received OSNR per carrier), the BERs of all the 11 carriers with hard decision and post-filter & MLSD are shown in Fig. 7. The 1st and 11th carriers subject to one-sided linear crosstalk exhibit lower BERs.

#161326 - $15.00 USD Received 11 Jan 2012; revised 23 Feb 2012; accepted 19 Mar 2012; published 19 Apr 2012

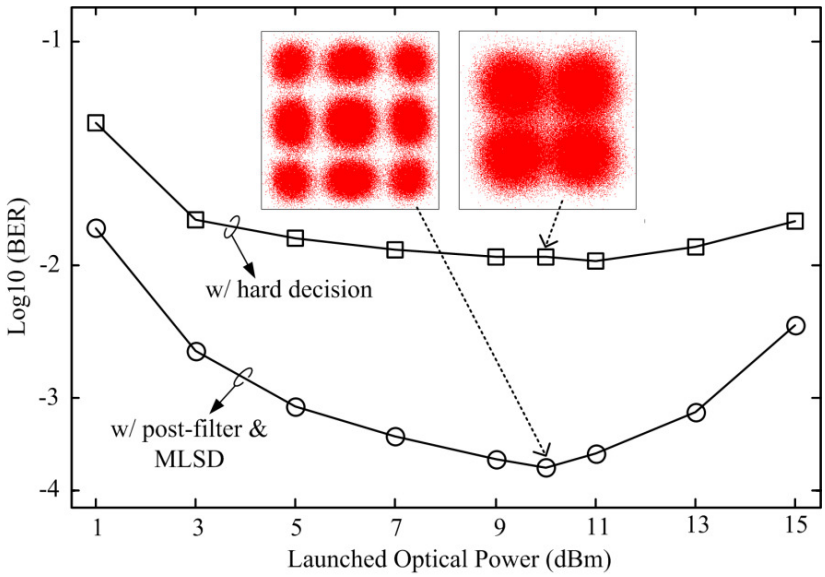

Fig. 6. Performance of 1.232 Tbit/s superchannel transmissions over 640 km SSMF as a function of launched power.

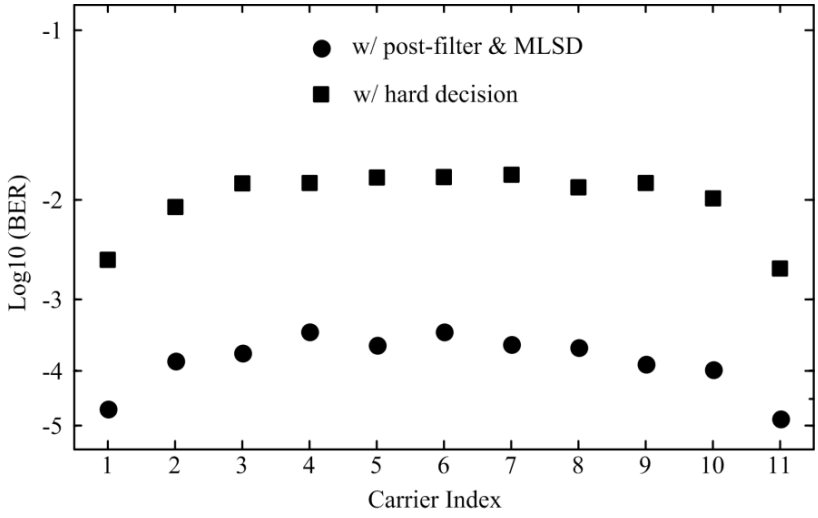

Fig. 7. The BERs of all the 11 carriers after 640 km SSMF transmission at 10 dBm launched total power.

3.4 Tolerance to concatenated WSSs

In future flexible optical networks, the Terabit superchannel is routed as a single entity over multiple reconfigurable optical add and drop multiplexers (ROADMs) in which the WSSs are basic building blocks. The tolerance to the concatenated WSSs of the proposed 1.232 Tbit/s superchannel solution is investigated in the subsection. Figure 8 shows the optical spectrum of the generated 1.232 Tbit/s 11-carrier superchannel signal and the transfer functions of a single 300 GHz WSS and 20 concatenated 300 GHz WSSs. The generated 1.232 Tbit/s superchannel has a 10-dB bandwidth of 280 GHz. It can also be observed that there is still an amount of filtering margin even if the superchannel signal passes through 20 concatenated 300 GHz WSSs. On the other hand, this filtering margin can also be interpreted as good tolerance to the

#161326 - $15.00 USD Received 11 Jan 2012; revised 23 Feb 2012; accepted 19 Mar 2012; published 19 Apr 2012

wavelength drift of the lasers. Therefore, the generated 1.232 Tbit/s superchannel can be well accommodated within six 50-GHz grids without need for additional guard bands.

The narrowband filtering effect induced by the concatenation of multiple WSSs mainly influence the most outer two carriers (i.e. 1st and 11th carriers). We swept the 3-dB bandwidth of WSS2 in Fig. 2 to emulate the narrowband filtering effect. When sweeping the bandwidth of WSS2, the launched power was set to be 10 dBm. The Q-penalties of 1st and 11th carriers are plotted in Fig. 9 as a function of the 3-dB bandwidth of WSS2. Given a Q-penalty within 0.5 dB, the two carriers can tolerant a filtering bandwidth of as low as 265 GHz.

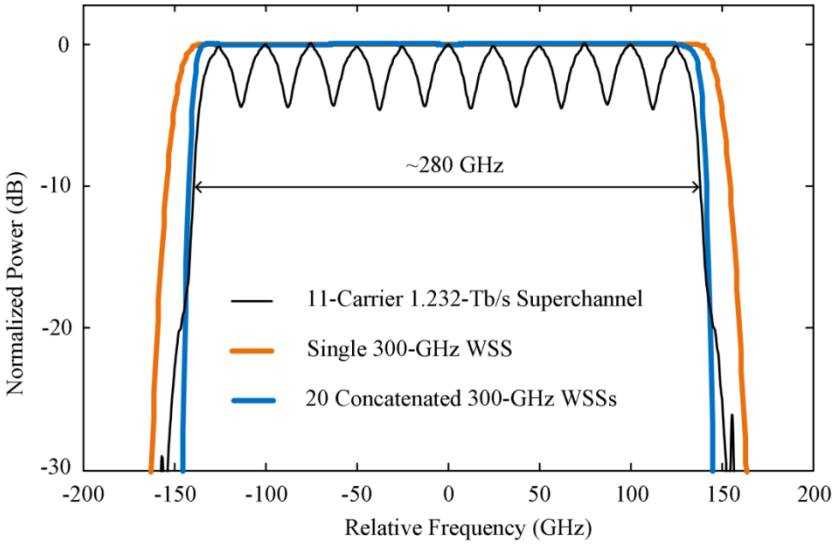

Fig. 8. The optical spectrum of the generated 1.232 Tbit/s RS-DBS-WDM superchannel and the transfer functions of a single 300 GHz WSS and 20 concatenated 300 GHz WSSs.

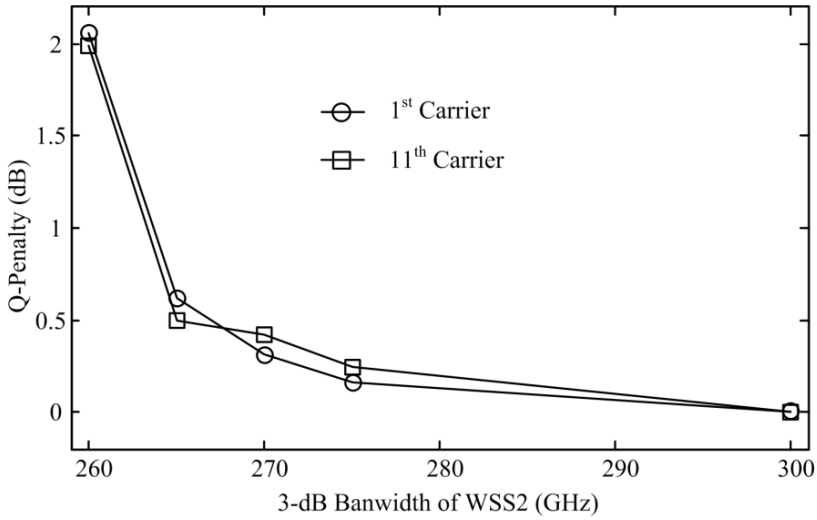

Fig. 9. The Q-penalties of 1st and 11th carriers as a function of the bandwidth of WSS2.

4. Complexity comparison of different solutions to building up superchannels

Table 1 compares the complexity of different solutions to building up multi-carrier superchannels. All the listed solutions can provide comparable spectral efficiency given an

#161326 - $15.00 USD Received 11 Jan 2012; revised 23 Feb 2012; accepted 19 Mar 2012; published 19 Apr 2012

identical modulation format. However, it is noteworthy that the proposed RS-DBS-WDM solution allows for an achievable spectral efficiency slightly above the Nyquist limit (e.g. 28 Gbaud w.r.t. 25 GHz in the above demonstrations) at the expense of larger implementation penalty due to stronger linear crosstalk. We evaluated these approaches themselves excluding the modulation format dependence. Coherent detection was assumed for all solutions.

Table 1. Comparison of Different Solutions to Building up Superchannels (H: high; M: medium; L: Low)

		Electro-Optic OFDM [1,2]	**NGI-OFDM** [3–6]	**Nyquist-WDM w/ Electrical Shaping** [8,9]	**Nyquist-WDM w/ Optical Shaping** [10,11]	**RS-DBS-WDM**
Tx	Electrical Complexity	H	L	H	L	L
	Optical Complexity	M	M	M	H	L
Rx	Electrical Complexity	M	L	L	L	M
	Optical Complexity	M	H	L	L	L

As for the electro-optic OFDM also called multi-band OFDM, the electrical transceiver complexity is high due to the required high-performance digital-to-analog converters (DACs)/ADCs in terms of their analog bandwidth, sampling speed, and effective quantization resolution. Furthermore, OFDM often requires a little more electrical complexity to handle the synchronization problem. The maintenance of the carrier orthogonality needs medium higher analog bandwidth of the transceivers as compared to WDM-based solutions. The additional temporal or spectral overheads reduce the net spectral efficiency.

The NGI-OFDM approach shifts most of the complexity from the electrical part to the optical part. However, both the electrical and optical complexity in the receivers is still in a high level owing to the high oversampling rate and analog bandwidth. The symbols in all the carriers are required to be time-aligned to guarantee the orthogonality. Large alignment deviation leads to high performance loss [23]. Another practical disadvantage of NGI-OFDM is the incompatibility to the WDM components (e.g. AWG) when combining the carriers together due to the stringent orthogonality demand. If the carrier count is relatively high, the entire transmitter will suffer from high insertion loss by replacing AWGs with *N*:1 optical couplers.

Regarding the Nyquist-WDM, there are two major ways to realize the desired rectangular spectral shape. Although the receiver complexity is similar to that in conventional WDM systems, they still burden either the optical or electrical complexity on the transmitter side. In [8,9], advanced DSP was applied in the transmitters with the help of high-performance DACs. The rectangular spectral shape can also be achieved in the optical domain by specific spectral shaping [10,11]. The later way often suffers from a larger implementation penalty due to the limited optical resolution while manipulating the optical spectrum. Anyway, it commonly takes much effort and complexity to realize rectangular spectra in both ways. Furthermore, the carrier spacing has to be slightly larger than the baud rate to ensure acceptable linear crosstalk due to the imperfect rectangular spectral shape in practical implementations. Similar to the NGI-OFDM approach, *N*:1 optical couplers are preferred to AWGs when combining the carriers together in order to keep the rectangular spectral shape. Thus, the resultant high insertion loss and low delivered OSNR would be problems.

In comparison, the complexity of RS-DBS-WDM approach is on the same level with the conventional WDM systems. Since RS-DBS-WDM allows for the existence of strong ISI and more compact signal spectra, the transceiver analog bandwidth is even smaller than that in conventional WDM systems. This helps to reduce the photonic integration effort or cost by using relatively low-end transceiver components. Due to the compatibility with the

#161326 - $15.00 USD Received 11 Jan 2012; revised 23 Feb 2012; accepted 19 Mar 2012; published 19 Apr 2012

conventional WDM configuration, it is convenient to form Terabit superchannels using already-commercial WDM components and engineering techniques. Although the hard decision circuits are substituted by the post-filter and MLSD in the receiver DSP part, the computational complexity of the post-filter and MLSD is small due to the short memory of duobinary response. Moreover, both the post-filter and MLSD format can be implemented without multiplications for QPSK (see Appendix) and with several reduce-state MLSD algorithms for higher-level quadrature amplitude modulation (See [28,29]). To summarize, the complexity increment imposed by the RS-DBS-WDM solution is low w.r.t. the conventional WDM systems.

5. Conclusion

In addition to OFDM and Nyquist-WDM, another attractive solution based on RS-DBS-WDM has been proposed and experimentally demonstrated to form spectrally-efficient Terabit superchannels. Given an identical modulation format, the RS-DBS-WDM approach can achieve higher spectral-efficiency than the other two approaches. There are a number of advantages of the proposed RS-DBS-WDM approach which facilitates a practical implementation, such as compatibility with the WDM components, high bandwidth efficiency, low implementation complexity, and comparable receiver sensitivity. In this paper, generation and transmission of a 1.232-Tbit/s 11-carrier PM-QPSK superchannel have been experimentally demonstrated based on RS-DBS-WDM. For the QPSK format, a multiplier-free MLSD algorithm was developed to further simplify the RS-DBS-WDM solution.

Appendix

As mentioned in the main text, MLSD is respectively implemented on the in-phase and quadrature paths of a duobinary-shaped QPSK signal (see Fig. 4). Since the signal on either in-phase or quadrature path is based on 2PAM, we describe the simplified MLSD algorithm on the basis of 2PAM as was done in [12].

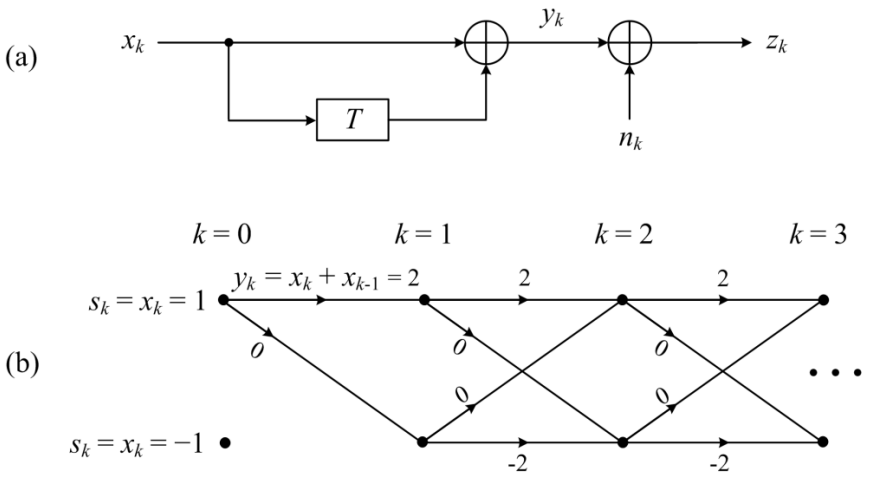

Fig. 10. (a) duobinary-shaped channel model with AWGN; (b) Trellis for duobinary-shaped 2PAM.

The trellis for duobinary-shaped 2PAM and the duobinary-shaped channel model in the presence of additive white Gaussian noise (AWGN) are shown in Fig. 10. Here, we denote

- x_k : the input 2PAM symbol in the k^{th} trellis stage or the k^{th} time slot. x_k takes two possible levels, i.e. $x_k \in \{1, -1\}$.

#161326 - $15.00 USD Received 11 Jan 2012; revised 23 Feb 2012; accepted 19 Mar 2012; published 19 Apr 2012

- s_k : the state in the k^{th} trellis stage. Since the memory length is one symbol for duobinary-shaped signal, s_k is directly given by x_k.
- y_k : the duobinary-shaped noiseless 2PAM symbol in the k^{th} trellis stage. y_k takes three possible levels, i.e. $y_k \in \{2, 0, -2\}$, since $y_k = x_k + x_{k-1}$.
- n_k : the AWGN sample in the k^{th} trellis stage.
- z_k : the received noisy signal in the k^{th} trellis stage. We have $z_k = y_k + n_k$.

In the k^{th} stage or time slot, the Viterbi algorithm computes several distance metrics for each state in a recursive way. The distance metrics for each state is given by [12]

$$DM\left(x_k\right) = \min_{x_{k-1}}\left\{ DM\left(x_{k-1}\right) + \Delta DM\left(x_{k-1}, x_k\right)\right\} = \min_{x_{k-1}}\left\{ DM\left(x_{k-1}\right) + \left(z_k - y_k\right)^2\right\}, \quad (1)$$

where $DM\ (x_k)$ denotes the distance metric assigned to state x_k in the k^{th} stage; $\Delta DM\ (x_{k-1}, x_k)$ denotes the distance metric increment corresponding to the trellis branch from x_{k-1} to x_k in the k^{th} stage. Since the entire distance metrics are all made up of the accumulated metric increments, we can only focus on the $\Delta DM\ (x_{k-1}, x_k)$ for notation convenience.

$$\Delta DM\left(x_{k-1}, x_k\right) = \left(z_k - y_k\right)^2. \quad (2)$$

In the Viterbi algorithm, comparisons between the distance metrics are required to determine the survivor path for each state in each stage. We can consider the differences between these distance metrics instead of the absolute metrics. This means we can add or subtract a constant over all the distance metrics at the same time without changing the comparison results. It can be seen from Eq. (2) that all the distance metric increments have a common term z_k^2 in the k^{th} stage. Thus, we can subtract z_k^2 from all the distance metric increments in each stage.

$$\Delta DM\left(x_{k-1}, x_k\right) = -2 y_k z_k + y_k^2. \quad (3)$$

Further, we can also divide a positive factor of 4 over all distance metric increments without changing the comparison results. Hence, we have

$$\Delta DM\left(x_{k-1}, x_k\right) = -\frac{1}{2} y_k z_k + \left(\frac{1}{2} y_k\right)^2. \quad (4)$$

Since y_k takes three possible levels, i.e. $y_k \in \{2, 0, -2\}$, $y_k / 2 \in \{1, 0, -1\}$. Then, we can represent the distance metric increment in the k^{th} stage as

$$\Delta DM\left(x_{k-1}, x_k\right) = \begin{cases} -z_k + 1 & y_k = 2 \\ 0 & y_k = 0 \\ z_k + 1 & y_k = -2 \end{cases}. \quad (5)$$

It can be seen that multiplier-free distance metrics can be used without any performance loss. For each 2PAM symbol, the MLSD merely involves 4 additions and 2 comparisons all over real numbers. In essence, the above derivation exploited both the inherent 2-level property of 2PAM signals and the one-symbol-delay-and-add duobinary pattern.

#161326 - $15.00 USD Received 11 Jan 2012; revised 23 Feb 2012; accepted 19 Mar 2012; published 19 Apr 2012